zac01216/zac5743d16z | xppws | S=1 | 10/18/16 | 23:43 | 4/C Fig: 1,2,3,4,5,6,7,8,9,10 | ArtID: 01586-16 | NLM: research-article | CE: jmm

Editor: Rice | Section: Susceptibility | Designation: T

AMERICAN SOCIETY FOR MICROBIOLOGY | Antimicrobial Agents and Chemotherapy

A Bioluminescent *Francisella tularensis* SCHU S4 Strain Enables Noninvasive Tracking of Bacterial Dissemination and the Evaluation of Antibiotics in an Inhalational Mouse Model of Tularemia

AQ: au Charlotte A. Hall,[a*] Helen C. Flick-Smith,[b] Sarah V. Harding,[b] Helen S. Atkins,[a,b] Richard W. Titball[a]

AQ: aff Bacterial Pathogenesis Research Group, College of Life and Environmental Sciences, University of Exeter, Exeter, United Kingdom[a]; CBR Division, Defence Science and Technology Laboratory, Porton Down, Salisbury, Wiltshire, United Kingdom[b]

Bioluminescence imaging (BLI) enables real-time, noninvasive tracking of infection *in vivo* and longitudinal infection studies. In this study, a bioluminescent *Francisella tularensis* strain, SCHU S4-*lux*, was used to develop an inhalational infection model in BALB/c mice. Mice were infected intranasally, and the progression of infection was monitored in real time using BLI. A bioluminescent signal was detectable from 3 days postinfection (3 dpi), initially in the spleen and then in the liver and lymph nodes, before finally becoming systemic. The level of bioluminescent signal correlated with bacterial numbers *in vivo*, enabling noninvasive quantification of bacterial burdens in tissues. Treatment with levofloxacin (commencing at 4 dpi) significantly reduced the BLI signal. Furthermore, BLI was able to distinguish noninvasively between different levofloxacin treatment regimens and to identify sites of relapse following treatment cessation. These data demonstrate that BLI and SCHU S4-*lux* are suitable for the study of *F. tularensis* pathogenesis and the evaluation of therapeutics for tularemia.

Francisella tularensis is a Gram-negative intracellular bacterium and is the etiological agent of the disease tularemia. Tularemia has a low infectious dose by the aerosol route (50% infectious dose [ID_{50}], <10 CFU), causing a disabling illness without rapid treatment, and is considered a potential biothreat agent. The preferred treatments for tularemia are limited to a few antibiotics, including fluoroquinolones (1, 2), tetracycline (3), streptomycin (4, 5), and gentamicin (6, 7). The lack of a licensed vaccine, reported treatment failures, even with preferred antibiotics (8), and a 2% mortality rate despite treatment (5) necessitate the development and evaluation of new therapies.

Conventional methods of assessing bacterial growth and dissemination *in vivo* require the infection of large cohorts of animals and the culling of groups of animals at set time points throughout a study. This strategy not only uses large numbers of animals but is also labor-intensive and subject to tissue sampling bias. Noninvasive imaging techniques, such as bioluminescence imaging (BLI), can report spatial and temporal aspects of infectious diseases *in vivo* both longitudinally and in real time (9). BLI typically relies on the detection of light produced by luciferase-catalyzed oxidation reactions, which are encoded in the pathogen of interest, by use of a sensitive charge-coupled device (CCD) camera (10). Pivotal experiments by Contag et al. have demonstrated the usefulness of BLI in the noninvasive study of bacterial pathogenesis and the evaluation of antibiotic treatments for *Salmonella enterica* serovar Typhimurium (11). Subsequently, bioluminescent reporters have been introduced into other bacteria, including *Mycobacterium tuberculosis* (10, 12), *Staphylococcus aureus* (13, 14), *Burkholderia mallei* (15), and *Yersinia pestis* (16, 17). Further, BLI has been used to evaluate vaccines (18), antibiotics (19–21), and supportive therapies (22) for a range of pathogens. BLI is noninvasive, allowing sequential imaging of the same animal and enabling the bacterial burden to be quantified without culling the animal, thus reducing animal usage. Moreover, because the entire animal is sampled, tissue sampling bias is reduced, and the identification of different foci of infection is possible. This has the potential to improve our understanding of disease progression and to aid in the development of better treatments. A bioluminescent live vaccine strain (LVS) of *F. tularensis* has been constructed previously (23). However, the plasmid encoding the luminescence was unstable *in vivo*, potentially leading to underestimation of the bacterial load. This would be a considerable limitation in the use of this strain to evaluate therapies. To date, no *in vivo* model has been reported for bioluminescent *F. tularensis* SCHU S4.

Here we describe the construction of a bioluminescent strain of *F. tularensis* SCHU S4 and demonstrate the suitability of this strain for tracking disease progression. The value of BLI for the evaluation of antibiotic treatment and the identification of sites of relapse of disease is also demonstrated.

MATERIALS AND METHODS

Bacteria. *Francisella tularensis* subsp. *tularensis* strain SCHU S4 was cultured on blood glucose cysteine agar (BCGA) plates or in modified cysteine partial hydrolysate (MCPH) broth supplemented with L-cysteine and glucose. Electroporation was used to transform plasmid pEDL41 (containing *luxCDABE*) into SCHU S4 by methods described previously (24), thereby constructing strain SCHU S4-*lux*. Bioluminescent strains were cultured with hygromycin B (200 μg ml^{-1}). All manipulations of *F.*

Received 20 July 2016 **Returned for modification** 16 August 2016
Accepted 8 September 2016

Accepted manuscript posted online 26 September 2016

Citation Hall CA, Flick-Smith HC, Harding SV, Atkins HS, Titball RW. 2016. A bioluminescent *Francisella tularensis* SCHU S4 strain enables noninvasive tracking of bacterial dissemination and the evaluation of antibiotics in an inhalational mouse model of tularemia. Antimicrob Agents Chemother 60:000–000. doi:10.1128/AAC.01586-16.

Address correspondence to Charlotte A. Hall, c.hall5@herts.ac.uk.

* Present address: Charlotte A. Hall, Research Centre in Topical Drug Delivery and Toxicology, University of Hertfordshire, Hatfield, United Kingdom.

Copyright © 2016, American Society for Microbiology. All Rights Reserved.

tularensis SCHU S4 and SCHU S4-*lux* were performed in a class III microbiological safety cabinet.

Bacterial growth *in vitro*. Bacteria were grown at 37°C in 96-well flat-bottom plates (200 μl per well) with a starting optical density at 595 nm (OD_{595}) of 0.02. Absorbance (expressed as OD_{595}) was measured every 30 min, using a plate reader capable of constant shaking, for 48 h. Each strain was plated into 6 replicate wells. Wells containing MCPH without bacteria served as medium controls.

Intracellular replication assay. Bacterial invasion and intracellular survival were studied in J774A.1 murine macrophage-like cells. The cells were seeded onto a 24-well tissue culture plate to give a concentration of 1×10^6 cells per well following overnight incubation in Dulbecco's modified Eagle's medium (DMEM) (Gibco Life Technologies) supplemented with 1% L-glutamine and 10% fetal calf serum at 37°C.

One milliliter of Leibovitz's L-15 medium (Gibco Life Technologies) containing 10^6 CFU of either SCHU S4 or SCHU S4-*lux* was added to cell monolayers to achieve a multiplicity of infection (MOI) of 1. Each strain was added to wells in triplicate for each time point. J774A.1 cells were incubated with bacteria at 37°C for 1 h, after which the medium was replaced with L-15 medium containing either 10 μg ml^{-1} gentamicin (for the 1-h-postinfection [1-hpi] time point) or 2 μg ml^{-1} gentamicin (for the 4- or 24-hpi time point). The cells were then reincubated at 37°C for 30 min, 4 h, or 24 h for the 1-, 4-, or 24-hpi time point, respectively. At these time points, the L-15 medium was removed and the cells lysed with 1 ml distilled water (dH_2O). The cell lysates were serially diluted in phosphate-buffered saline (PBS) and were plated onto BCGA plates in triplicate in order to determine the intracellular bacterial load. The actual MOI was determined by serially diluting the inoculum in sterile PBS and plating onto BCGA plates. For SCHU S4-*lux*, cell lysates were plated onto BCGA plates with or without hygromycin B in order to determine plasmid stability by comparing the bacterial numbers on selective and nonselective agars.

Animals. All studies involving animals were performed in accordance with the requirements of the Animal (Scientific Procedures) Act 1986. Six- to 8-week-old female BALB/c mice were obtained from Charles River Laboratories and were randomly allocated to cages of five mice each upon arrival. The mice were implanted with microchips prior to arrival to enable the identification of individuals. The animals were housed within a rigid-wall half-suit class III isolator with access to food and water *ad libitum* and a 12-h light-dark cycle.

Following infection with *F. tularensis*, animals were handled under ACDP (Advisory Committee for Dangerous Pathogens) containment biosafety level III conditions for imaging studies (25). Mice were weighed daily and were observed twice daily for clinical signs of disease. Upon reaching predetermined humane endpoints, mice were culled by cervical dislocation.

AQ: A

Bacterial challenge. Mice were infected by the intranasal route with either *F. tularensis* SCHU S4 or SCHU S4-*lux*, both of which were prepared by diluting frozen 10% sucrose stocks. For the bacterial challenge, mice were briefly anesthetized using isoflurane within a bell jar and were inoculated with approximately 10^3 CFU in a total volume of 50 μl PBS (25 μl per naris). Serial dilution of the challenge dose and subsequent plating onto BCGA plates in triplicate determined the actual CFU given.

Bioluminescent imaging. The IVIS Spectrum system (PerkinElmer) measured the bioluminescent signal intensities during the imaging study using an open emission filter with exposure times adjusted to collect between 600 and 60,000 counts. Two-dimensional images had the background signal subtracted, and image scaling was normalized by converting total counts to photons per second. Bioluminescent signal intensity is represented by a pseudocolor scale ranging from red (most intense) to violet (least intense). Signal intensity images were superimposed over grayscale reference photographs for anatomical registration. Scales were manually set to the same values for comparable images to normalize the intensity of the bioluminescence across time points. Bioluminescence within specific regions of individual animals was quantified using the region-of-interest (ROI) tool in Living Image software, version 4.5 (PerkinElmer).

Mice were anesthetized for imaging with 40 mg ketamine (Vetalar; Zoetis) kg of body $weight^{-1}$ and 0.75 mg medetomidine (Domitor; Vetoquinol) kg of body $weight^{-1}$, administered by the intraperitoneal route in 150 μl sterile water. Mice were housed in a heated box to prevent hypothermia during the anesthetic process. Anesthesia was reversed using 2.5 mg atipamezole (Antisedan; Zoetis) kg^{-1}, administered by the intraperitoneal route in 100 μl sterile water. The mice remained in a heated box until fully recovered. All mice were shaved (dorsum and abdomen/thorax) under anesthesia prior to challenge in order to reduce signal absorption by the fur. Shaved mice had a recovery period of at least 24 h before challenge.

Quantification of *F. tularensis in vivo*. The relationship between the intensity of the bioluminescent signal and the bacterial burden in organs was determined in order to allow noninvasive bacterial quantification *in vivo*.

The *in vivo* bioluminescent signal was measured daily by imaging groups of five mice under terminal anesthesia. Organs (lungs, liver, and spleen) were aseptically removed from culled mice and were imaged *ex vivo*. Groups of five mice were also inoculated with the parent strain, SCHU S4, to provide a benchmark by which the fitness of the SCHU S4-*lux* strain could be assessed.

The bacterial burden was determined by homogenizing organs in 1 ml PBS using a cell sieve and plating serial dilutions of tissue homogenates onto BCGA plates. *In vivo* plasmid stability was measured by plating tissue homogenates from mice challenged with SCHU S4-*lux* onto BCGA plates in triplicate with and without hygromycin B in order to calculate the ratio of hygromycin-resistant to hygromycin-sensitive bacteria. Agar plates were also imaged using the IVIS Spectrum system to confirm that the bacteria isolated from the organs had retained the plasmid containing the *lux* operon.

Antibiotic dosing schedule. Groups of 10 mice infected intranasally with SCHU S4-*lux* were randomized to receive either (i) PBS, (ii) levofloxacin at 40 mg kg^{-1}, or (iii) levofloxacin at 5 mg kg^{-1}. All treatments were administered intraperitoneally once daily for 7 days, starting at 4 days postinfection (4 dpi). Groups of animals ($n = 5$) inoculated intranasally with SCHU S4-*lux* and receiving no treatment or sham challenged with PBS were also included. Animals were monitored for 18 days after the discontinuation of therapy in order to image any relapse.

Mice were imaged at regular intervals from 3 dpi until the end of the study. To determine if repeated anesthesia affected antibiotic efficacy or survival, groups of infected mice receiving antibiotics only were included. These animals were not imaged during the study, but organs were harvested and imaged postmortem (as above). At the end of the study (or once mice had reached a predetermined humane endpoint), the mice were terminally anesthetized, imaged, and culled. Organs (lungs, liver, and spleen) from all mice were aseptically removed and were imaged prior to processing for bacterial enumeration.

Statistical analysis. GraphPad Prism software, version 6, was used for all statistical analysis and the production of all graphs. Differences in survival data were analyzed using a log rank (Mantel-Cox) test. CFU data were log transformed to fit the requirements for parametric analysis. Statistical differences between two groups were determined using an unpaired *t* test. Statistical differences between three or more groups were determined using one-way analysis of variance (ANOVA) followed by a Bonferroni multiple-comparison test. To determine the relationship between CFU and bioluminescent signal intensity, data were log transformed and a Pearson two-tailed correlation test was performed. R^2 values were calculated using linear regression analysis. Growth curves were compared by log-transforming data and performing nonlinear regression analysis. Two-way ANOVA with Sidak's multiple-comparison test revealed which time points were significantly different. Significance was predetermined at a *P* value of ≤ 0.05.

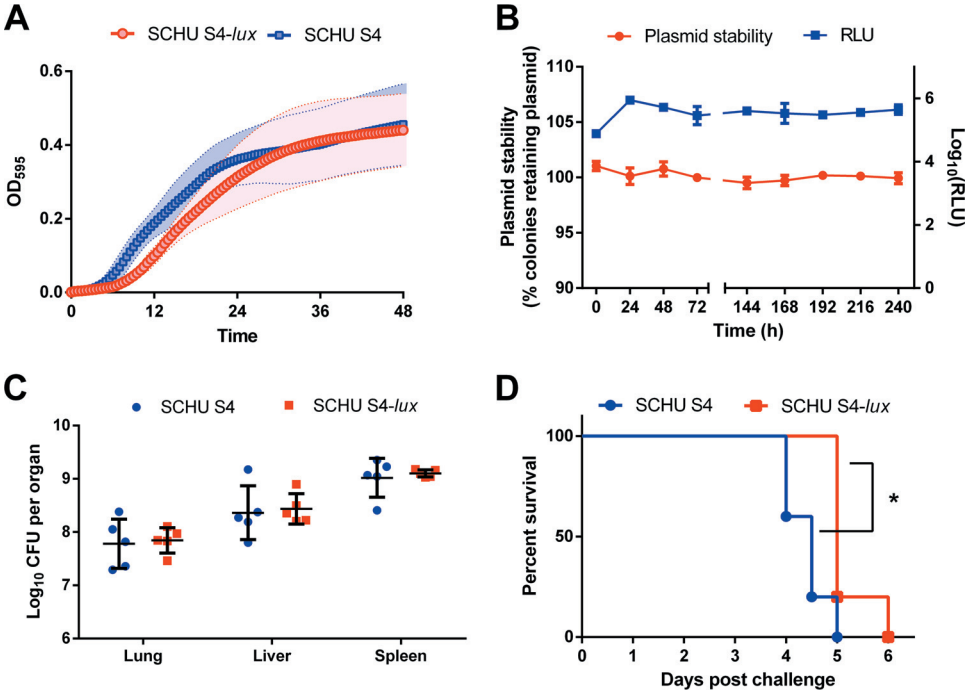

COLOR

FIG 1 Lux-marked SCHU S4 is stably replicated and virulent, but the lag phase of growth and the time to death are longer than those for SCHU S4. To determine if the *lux* reporter impacted SCHU S4 fitness, SCHU S4-*lux* was compared to SCHU S4 with regard to *in vitro* growth (3 separate experiments with 6 technical replicates per experiment) (A), bacterial burdens in organs (n, 5 animals per group) (C), and survival in a BALB/c mouse model (n, 5 animals per group) (D). The asterisk indicates a P value of 0.05. (B) *In vitro* plasmid stability and bioluminescence were also measured in the absence of antibiotic selective pressure (3 separate experiments with 3 technical replicates per experiment). The data shown represent mean values ± standard deviations.

RESULTS

SCHU S4-*lux* has an increased lag phase but is still virulent. *In vitro* growth during the lag phase was significantly slower for SCHU S4-*lux* than for the wild-type strain, SCHU S4, with a significant increase in the time to an OD_{595} value of 0.02 (Fig. 1A). F1 However, the log phases for the two strains were similar, and no significant difference in mean generation time was observed (data not shown). Moreover, the plasmid was stably retained following repeated subculturing in nonselective broth; >99% of colonies retained the plasmid after 10 days (Fig. 1B). Mortality was 100% for animals challenged with either SCHU S4 or SCHU S4-*lux*; the median times to death were 4 and 5 days for the SCHU S4 and SCHU S4-*lux* groups, respectively (Fig. 1D). Bacterial loads at the time of death were equivalent for animals challenged with either strain by the intranasal route (n = 5) (Fig. 1C), indicating that despite the difference in the lag phase of infection, the overall ability of SCHU S4-*lux* to disseminate and replicate intracellularly was not diminished. All animals in the PBS sham challenge group survived until the end of the study and displayed no clinical signs of infection (data not shown).

The bioluminescent signal is detectable with the onset of clinical signs in an intranasal model of *F. tularensis* infection. To determine if the bioluminescent signal was detectable *in vivo*, groups of five mice were infected intranasally with approximately 10^3 CFU of SCHU S4-*lux*. At 3 dpi, the mice displayed no clinical signs of infection, and no bioluminescent signal was detected (Fig. F2/AQ:B 2). However, bioluminescent signals were detected from the explanted lungs of 3 out of 5 mice (Fig. 3). By 4 dpi, mice displayed F3 mild clinical signs—namely, various degrees of fur ruffling—and bioluminescent signals were detected in the spleens (Fig. 2); the anatomical location of the signal was confirmed by imaging the explanted organs (Fig. 3). During the primary infection, the bioluminescent signal spread from the spleen to the lymph nodes and liver before becoming systemic, with signal detectable in the lungs by 5 dpi (Fig. 2). The increase in bacterial loads seen between 3 dpi and 5 dpi occurred more rapidly in the spleens (4.3 log units) and livers (3.9 log units) than in the lungs (1.6 log units) (Fig. 4). No F4 bioluminescent signal was detected in mice challenged with the parent strain, SCHU S4, or with PBS at any time point (images not shown).

The level of bioluminescent signal (total flux) correlates with bacterial numbers *in vivo*. The relationship between the bacterial burden and the bioluminescent signal was established in order to determine whether BLI would allow noninvasive quantification of bacterial loads. The relationship between signal depth and signal attenuation by tissue required detection limits to be determined separately for the lungs, liver, and spleen.

There was a strong positive correlation between *in vivo* bioluminescence (expressed as total flux, in photons per second) and bacterial burdens in the lungs, livers, and spleens (Fig. 5). The F5 detection limit was calculated using linear regression analysis, with the detection threshold set at twice the average background signal measured in the wild-type group for each organ (Fig. 5). The calculated limits of detection were 6.46, 4.85, and 5.51 $\log_{10}$ CFU for the lungs, liver, and spleen, respectively, based on groups of 15 animals.

Noninvasive imaging is a sensitive measure of treatment efficacy at early time points. The utility of BLI for distinguishing

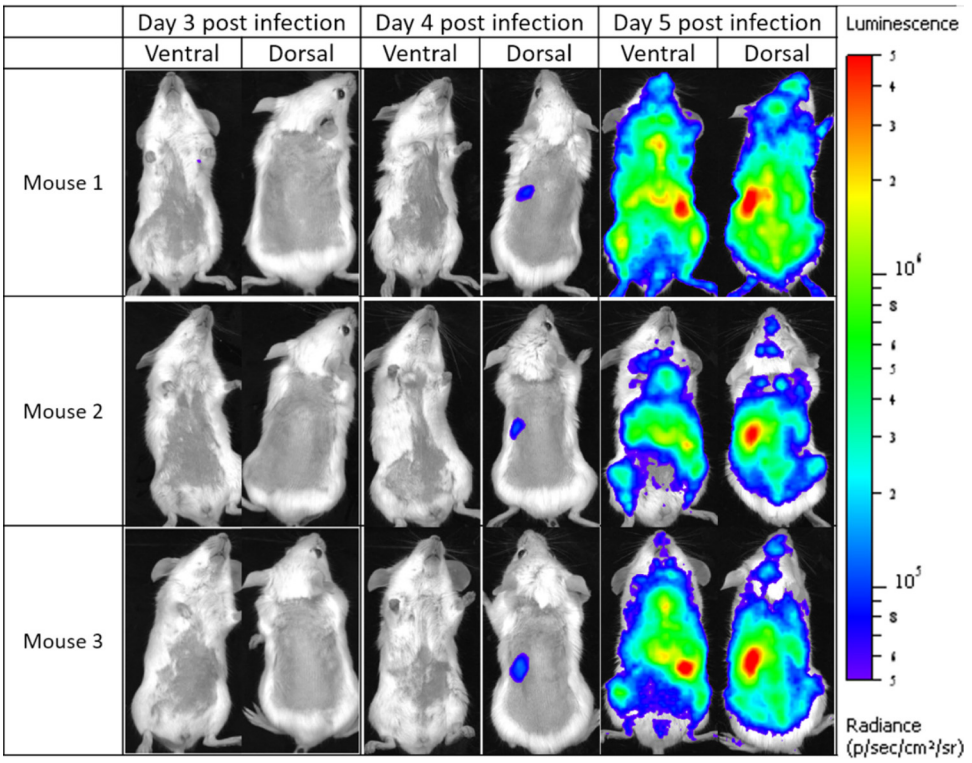

COLOR

FIG 2 *In vivo* imaging of BALB/c mice infected with SCHU S4-*lux* by the intranasal route. On days 3 to 5 postinfection, mice were terminally anesthetized and were imaged in ventral and dorsal alignments. The images shown are representative of groups of 5 mice at each time point. The intensity of photon emission is represented by pseudocolor images. The scale from blue to red represents low to high radiance efficiency (expressed as photons per second per square centimeter per steradian), respectively.

between different treatment regimens was assessed in a suboptimal antibiotic model. Groups of mice (n, 5 to 10) were infected intranasally with approximately 10^3 CFU of SCHU S4-*lux*. Levofloxacin (at 5 mg kg^{-1} or 40 mg kg^{-1}) or PBS was administered intraperitoneally once daily for 7 days, at the onset of a bioluminescent signal at 4 dpi (Fig. 6).

AQ: C
F6

At 5 dpi, the bioluminescent signal was diminished in both groups of mice receiving levofloxacin (n, 10 per group) (Fig. 6). The bioluminescent signal was below the limit of detection by 6 and 7 dpi for the groups dosed with 40 mg kg^{-1} and 5 mg kg^{-1} levofloxacin, respectively. Animals in the 5-mg kg^{-1} levofloxacin group had significantly higher total flux values in the thoracic and abdominal regions than animals in the 40-mg kg^{-1} levofloxacin group at 5 and 6 dpi (Fig. 7). No significant differences in other noninvasive parameters, including weight loss and clinical scores, were found between the two levofloxacin-dosed groups during the same period (Fig. 7). In SCHU S4-*lux*-infected animals receiving either PBS treatment or no treatment, the bioluminescent signal increased over the duration of the experiment until the animals

F7

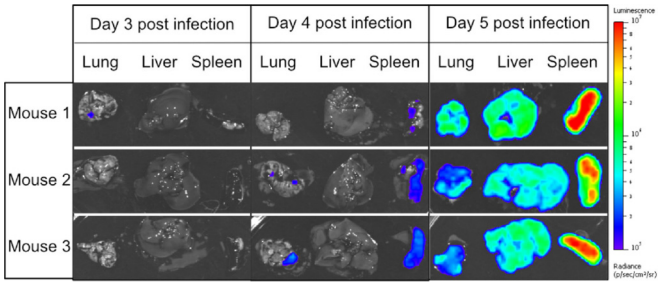

COLOR

FIG 3 *In vivo* bioluminescent signal quantification in BALB/c mice infected with SCHU S4-*lux* by the intranasal route. On days 3 to 5 postinfection, mice were terminally anesthetized, imaged, and culled following image acquisition, and organs (lungs, liver, and spleen) were aseptically removed and individually imaged. The images shown are representative of groups of 5 mice at each time point. The intensity of photon emission is represented by pseudocolor images. The scale from blue to red represents low to high radiance efficiency (expressed as photons per second per square centimeter per steradian), respectively.

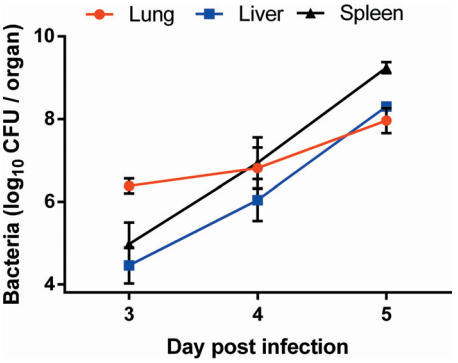

COLOR

FIG 4 SCHU S4-*lux* growth is slower in the lungs than in the spleen and liver. Groups of mice (n = 5) infected with 10^3 CFU of SCHU S4-*lux* were culled at 3, 4, and 5 dpi. The bacterial loads in the lung, liver, and spleen were determined by plating organ homogenates onto BCGA plates. Bacterial numbers are reported as total CFU for each organ. Data represent mean values ± standard deviations.

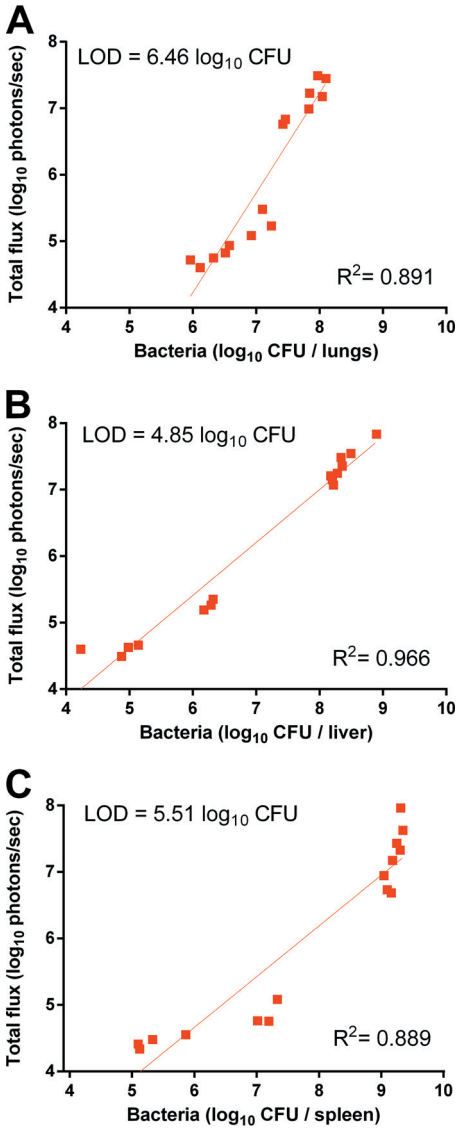

FIG 5 The intensity of the bioluminescent signal strongly correlates with bacterial loads in organs. Shown are the correlations between the levels of the bioluminescent signal detected and the numbers of bacteria in lungs (A), livers (B), and spleens (C) removed from mice infected with 10^3 CFU of SCHU S4-*lux* ($n = 15$). The bioluminescent signal (expressed as total flux) was measured for regions of interest corresponding to specific anatomical areas. The limits of detection (LOD) were calculated for each organ using linear regression analysis with the detection threshold set at twice the average background signal. Data points represent individual animals.

reached humane endpoints (Fig. 6). PBS treatment had no impact on the level of the bioluminescent signal; similar total flux values were observed for the PBS-treated and untreated groups (Fig. 6).

Noninvasive imaging identifies sites of relapse. Animals were monitored and imaged for 18 days after the completion of therapy in order to determine sites of relapse of infection. No bioluminescent signal was detected in animals treated with 40 mg kg^{-1} levofloxacin ($n = 10$). While bacteria were detected in spleen homogenates from these animals, no bacteria were detected in 22% and 33% of lung and liver samples, respectively (Fig. 8). However, 1 of 10 animals in the group dosed with 5 mg kg^{-1} levofloxacin showed clinical signs of relapse that subsequently resulted in a lethal infection. In this animal, the bioluminescent signal was below the limit of detection at the completion of antibiotic therapy, but by 14 dpi (3 days after the end of therapy), bioluminescence was evident in the intestinal region (Fig. 9). The bioluminescent signal continued to increase and spread from the intestinal region to the lungs and lymph nodes. By day 16 postinfection, the animal had succumbed to infection; the strongest bioluminescent signal was detected in the lung postmortem (Fig. 8). Strong foci of signal were detected *ex vivo* in the colon region of the intestines, presumably in Peyer's patches (Fig. 10). Foci of bioluminescence in the intestines were also observed postmortem in animals in the nonimaged group dosed with 5 mg kg^{-1} levofloxacin.

DISCUSSION

This study used a plasmid-based approach to generate a bioluminescent strain of SCHU S4 suitable for real-time visualization and quantification of pulmonary tularemia using BLI. The incorporation of luciferase-encoding plasmids into bacteria is a common approach for the development of bioluminescent reporter strains (26). Chromosomally integrated luciferases are often preferred (27), because they are more stable than plasmid-based reporters, although sensitivity is generally lower (17, 28). It is recognized that plasmid-based reporters may be unstable *in vivo* in the absence of antibiotic selection (23, 29, 30). However, this study demonstrates that pEDL41 is stably maintained in the absence of antibiotic selection, both *in vitro* and *in vivo*. This plasmid is derived from the pFN10 family of *Francisella* shuttle vectors carrying *orf4* and *orf5* (31). Based on the homology of *orf5* with the *axe* (32) and *phd* (33) antitoxins, *orf4* and *orf5* are thought to encode components of a plasmid addiction system which likely improve plasmid retention *in vivo* and *in vitro* (13). In this study, the concentration of bacteria required to generate a detectable signal *in vivo* was relatively high, which may have limited the detection of bacteria very early in infection. However, this did not present a problem when imaging was performed at later time points in the infection, and our method allowed for treatment failure and relapse of infection to be visualized. Approaches to improving sensitivity could include the use of other reporters, such as red-shifted firefly luciferase, which have a lower metabolic burden (10, 34).

A significant difference in time to death was observed between mice infected with SCHU S4-*lux* and those infected with the parental wild-type strain, SCHU S4. However, there was no difference in mortality between these groups of animals. These *in vivo* findings might reflect the longer lag growth phase seen *in vitro* for SCHU S4-*lux* than for SCHU S4 and the similarity of the growth rates and cell densities of the strains in the exponential- and stationary-growth phases. This altered growth profile of SCHU S4-*lux* could be attributed to the early loss of the plasmid in the absence of antibiotic selective pressure. However, plasmid stability was calculated as ≥99% in bacteria repeatedly subcultured in nonselective broth as well as in bacteria isolated from organs, suggesting that the extended lag phase did not simply reflect plasmid loss.

Studies using *S.* Typhimurium have shown increased global gene expression during the lag phase, with upregulation of nucleotide metabolism and fatty acid biosynthesis (35). Therefore, it is hypothesized that the substrate and energy requirements of producing a bioluminescent signal would compete with the energy requirements for growth and would thus compromise the adap-

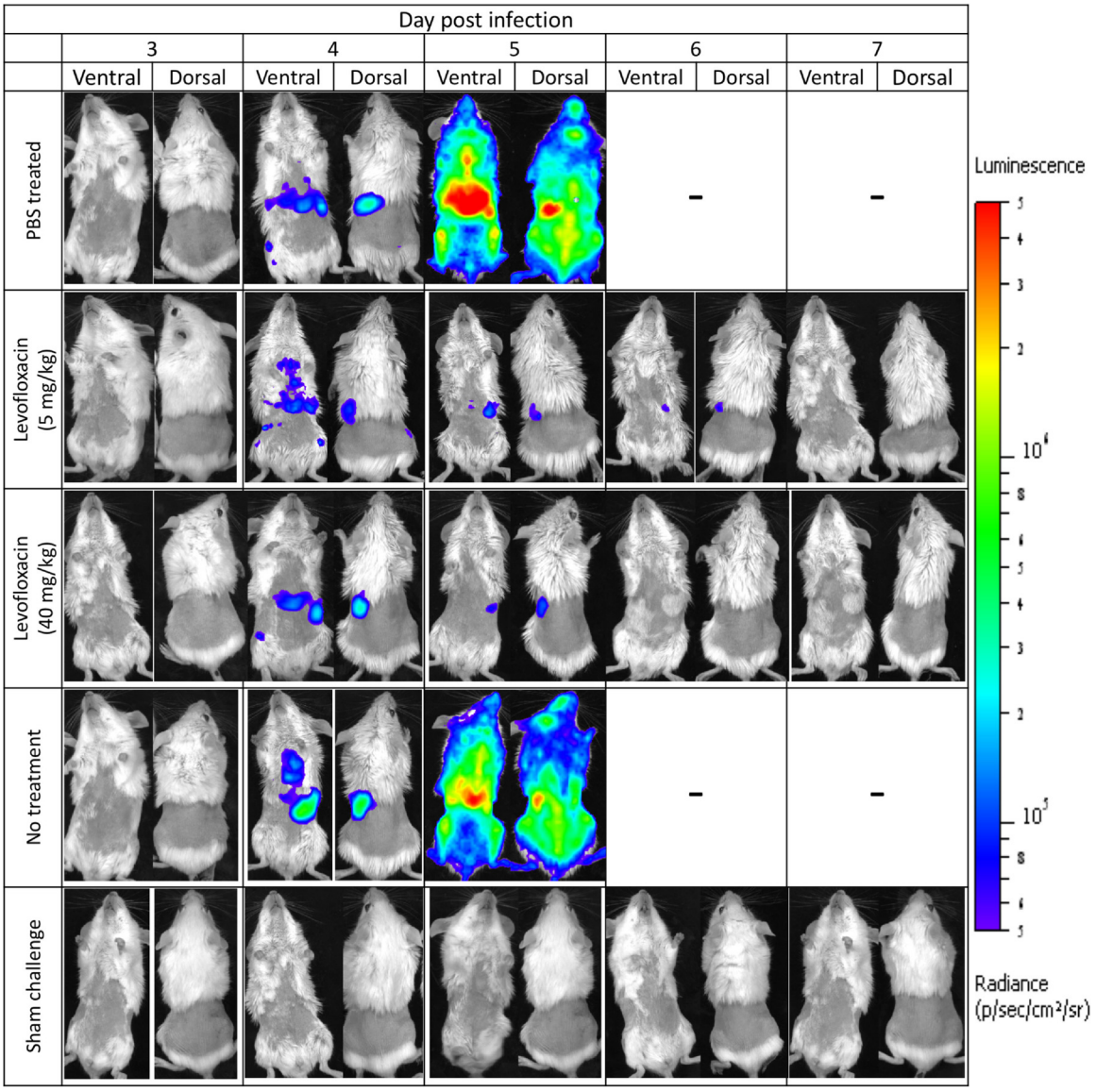

COLOR

FIG 6 Noninvasive optical imaging can be used to distinguish visually between different antibiotic regimens. Mice infected with 10^3 CFU SCHU S4-*lux* were treated with either PBS, 5 mg kg^{-1} levofloxacin, or 40 mg kg^{-1} levofloxacin administered by the intraperitoneal route and were imaged before, during, and after treatment. Representative images are shown for one mouse per group (*n*, 10 mice each in the PBS and levofloxacin treatment groups). Additionally, control groups of mice receiving either an SCHU S4-*lux* challenge or a PBS sham challenge but no further treatment were included (*n*, 5 mice each in the no-treatment and sham challenge groups). Image scaling was normalized by converting total counts to photons per second. The intensity of photon emission is represented by pseudocolor images. The scale from blue to red represents low to high radiance efficiency (expressed as photons per second per square centimeter per steradian), respectively.

tation of bacterial cells during the lag phase. A number of published studies have documented the level of attenuation that *luxCDABE* expression causes in bacteria. Impaired growth *in vitro* as a function of light intensity has been reported for some bioluminescent *Vibrio* species (36) and for *Streptococcus pyogenes* (29). In addition, a competitive disadvantage at the site of infection *in vivo* has been reported for *S. pyogenes* (29) and *Citrobacter rodentium* (37).

AQ: D

This study builds on previously reported BLI studies using a bioluminescent strain of *F. tularensis* LVS in mice (23, 38) and highlights the differences in pathogenesis between strains of differing virulence. Following an intranasal challenge with LVS-*lux*, bioluminescence was detected first in the lungs at 1 dpi and then in the lymph nodes, spleen, and liver by 3 or 4 dpi (23, 38). However, in our study, the bioluminescent signal was initially detected in the spleen at 4 dpi following an intranasal infection with 10^3 CFU. The bioluminescent signal could then be detected in the lymph nodes and liver before becoming systemic; the signal was not detected in the lungs until 5 dpi. The differences in the location and spread of signal between LVS-*lux* and SCHU S4-*lux* could be due to the differences in the challenge doses used. Infecting with a higher dose (5×10^5 to 1×10^6 CFU) of LVS-*lux* may have enabled earlier detection in the lungs than was observed after challenge with 10^3 CFU of SCHU S4-*lux*.

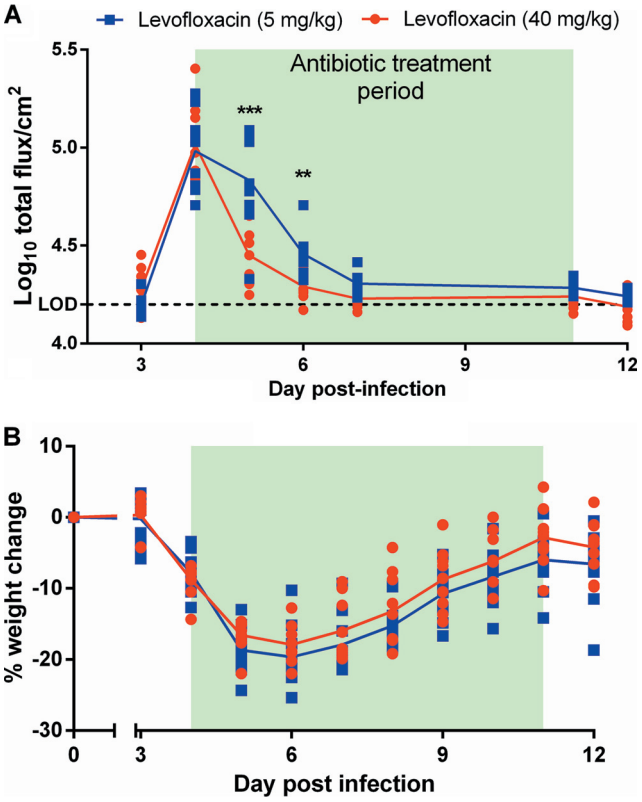

FIG 7 Mice receiving different doses of levofloxacin can be distinguished by the bioluminescent signal, but not by weight loss, early in antibiotic treatment. (A) Total flux from the thoracic and abdominal regions (normalized by area, in square centimeters) was measured and plotted over time for animals receiving either 5 mg kg^{-1} or 40 mg kg^{-1} levofloxacin. The dashed horizontal line indicates the limit of detection (LOD). (B) Animal weights were recorded daily and were plotted as the percentage of weight change relative to prechallenge weights. The data shown represent mean values ± standard deviations (n, 10 mice per group). Double and triple asterisks indicate P values of ≤0.01 and ≤0.001, respectively.

Early detection of bioluminescence in the lung may be hindered by a number of factors. Differences in the ability to image infection in different organs may reflect the anatomical location of the organ within the animal, since signal intensity is inversely proportional to signal depth (39). Therefore, the limit of detection in the lung was approximately 1 to 1.5 log units higher than the limit of detection in the spleen or liver. Additionally, the proximity of the lungs to the heart could further reduce signal intensity, since oxy- and deoxyhemoglobin absorb light wavelengths between ~400 and 600 nm (40), and attenuation of the bioluminescent signal emitted from bacteria located in the lungs has been reported for other pathogens (41).

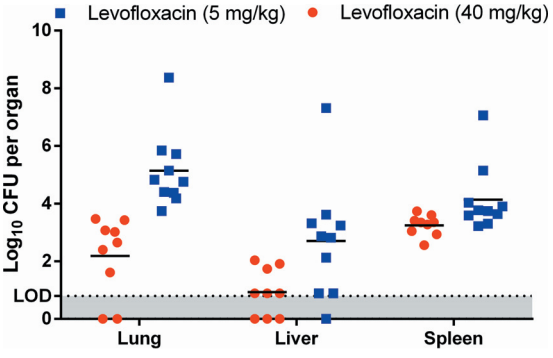

FIG 8 Bacterial clearance is not achieved following delayed antibiotic treatment. Groups of mice (n = 10) infected with SCHU S4-*lux* received either 5 or 40 mg kg^{-1} of levofloxacin by intraperitoneal injection. Bacterial loads for the lungs, liver, and spleen were determined by plating organ homogenates onto BCGA plates. The limit of detection (LOD) is indicated. Bacterial numbers are reported as the total CFU for each organ. Individual data points are plotted, and the central line for each group represents the mean value.

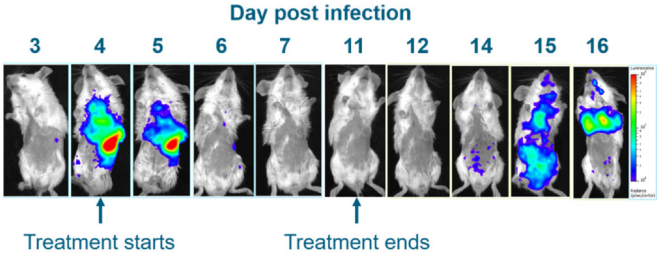

FIG 9 Noninvasive imaging enables the visualization of antibiotic efficacy. Mice were imaged before the start of antibiotic treatment (days 3 and 4), during treatment, and up to 18 days after the cessation of treatment. Shown is the infection course of one mouse in the suboptimal antibiotic treatment group (5 mg kg^{-1} levofloxacin). The bioluminescent signal decreases below the limit of detection following antibiotic treatment. Treatment was terminated on day 11, and a bioluminescent signal was detected in the intestinal region by day 15, indicating a relapse that progresses to a lethal infection, with a strong signal in the lungs.

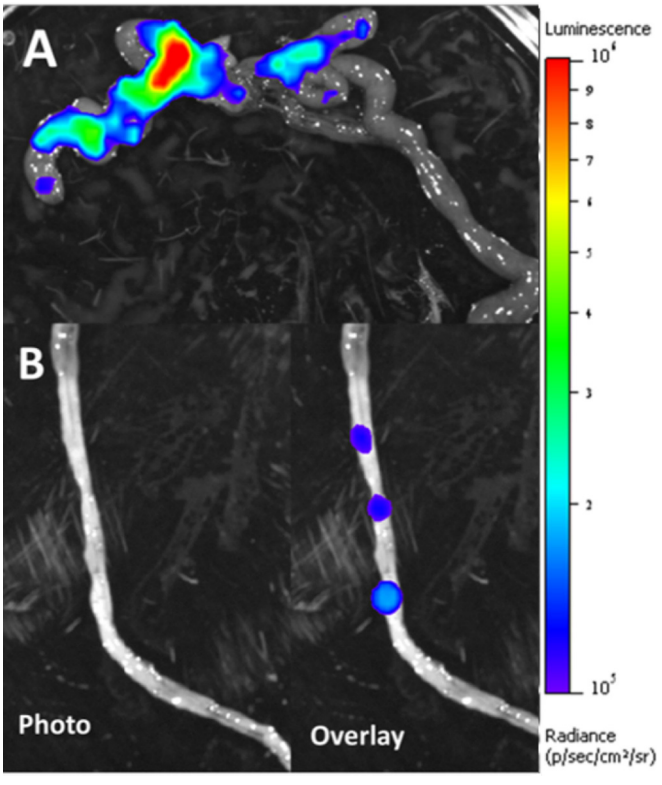

FIG 10 Bioluminescence imaging can assist in identifying sites of infection. (A) Bioluminescence was detected in the intestines of all relapsing mice. Shown are representative images from one of five relapsing mice. (B) Discrete foci of bioluminescent signal were observed in regions that did not otherwise show any gross pathology and that are presumed to be Peyer's patches.

AQ: F
AQ: G

The progression of infection visualized using BLI correlated with the bacterial load data from the organs; more-rapid increases in CFU counts were seen in the spleen (4.3 log units) and liver (3.9 log units) than in the lungs (1.6 log units) between 3 and 5 dpi. The kinetics of bacterial growth in different organs observed in this study are in agreement with those in previous studies, where bacteria grew more slowly in the lungs than in the liver and spleen following an intranasal challenge (42–44). Overall, these BLI data support the idea that it is widespread sepsis and systemic inflammation, rather than the primary pneumonia, that contribute to mortality (45–47).

Relapse following the withdrawal of antibiotics has been reported clinically (4, 5) and in experimental animals infected with *F. tularensis* (43, 48–50). In this study, the initiation of treatment was delayed until 4 dpi, and following the cessation of antibiotics, relapse was observed in 30% of the animals treated with 5 mg kg^{-1} levofloxacin. The relapse rate in this study is broadly similar to that reported previously (43). BLI enabled the tracking of infection during relapse and revealed that a bioluminescent signal could be detected in the gastrointestinal tract 3 days after the cessation of antibiotic therapy, before the detection of a signal in the thoracic cavity. After a mouse succumbed to the infection at 16 dpi (5 days following the termination of therapy), a bioluminescent signal was localized to discrete foci of infection within the intestines associated with lymphoid tissue, presumed to be Peyer's patches. It is possible that this represents a site of persistence from which the infection can be reestablished, since persistence in and dissemination from the gastrointestinal tract, specifically the Peyer's patches, has been widely reported for other pathogens with an intestinal tropism, including *Bacillus anthracis* (41), *Yersinia pseudotuberculosis* (51), *Mycobacterium avium* subsp. *paratuberculosis* (52), and *Listeria monocytogenes* (53). In another study, Ojeda et al. reported early trafficking of *Francisella novicida* to the gastrointestinal tract following infection by both the intranasal and intratracheal routes, with viable bacteria detected in the Peyer's patches (54). Following subcutaneous infection of field voles with *F. tularensis* subsp. *holarctica*, both intracellular and extracellular bacteria were detected in Peyer's patches as well as in intestinal epithelial cells (55). Thus, there is a growing body of data suggesting that *Francisella* is able to colonize Peyer's patches and that, as with other pathogens, persistence in and dissemination from the gastrointestinal tract may contribute to pathogenesis.

The reemergence of a bioluminescent signal in the lungs of SCHU S4-*lux*-infected mice could indicate bacterial trafficking from the gut to the lungs. Pneumonia resulting from bacterial translocation via the gut-lung axis has been reported for other pathogens, including *L. monocytogenes* (53) and *Streptococcus pneumoniae* (56). Additionally, the gastrointestinal microbiota plays a role in regulating bacterial translocation, and treatments that disrupt microbiota dynamics, such as antibiotics, may increase bacterial translocation (57). Further work is needed to determine the spatiotemporal population dynamics during relapse of infection with *F. tularensis* SCHU S4 and to determine whether different subpopulations of bacteria are responsible for the reemergence of infection in different organs, as noted previously for persistent *Salmonella* infections (58, 59).

ACKNOWLEDGMENTS

We thank Tom Kawula, UNC at Chapel Hill, for providing the pEDL41 plasmid.

C.A.H. carried out the experiments and drafted the manuscript. H.C.F.-S. assisted with the imaging experiments. R.W.T., S.V.H., and H.S.A. contributed to the study design and revised the manuscript. All authors read and approved the final manuscript.

We have no competing interests.

REFERENCES

1. **Johansson A, Berglund L, Gothefors L, Sjöstedt A, Tärnvik A.** 2000. Ciprofloxacin for treatment of tularemia in children. Pediatr Infect Dis J **19:**449–453. http://dx.doi.org/10.1097/00006454-200005000-00011.
2. **Limaye AP, Hooper CJ.** 1999. Treatment of tularemia with fluoroquinolones: two cases and review. Clin Infect Dis **29:**922–924. http://dx.doi.org/10.1086/520458.
3. **Overholt EL, Tigertt WD, Kadull PJ, Ward MK, Charkes ND, Rene RM, Salzman TE, Stephens M.** 1961. An analysis of forty-two cases of laboratory-acquired tularemia. Treatment with broad spectrum antibiotics. Am J Med **30:**785–806.
4. **Enderlin G, Morales L, Jacobs RF, Cross JT.** 1994. Streptomycin and alternative agents for the treatment of tularemia: review of the literature. Clin Infect Dis **19:**42–47. http://dx.doi.org/10.1093/clinids/19.1.42.
5. **Evans ME, Gregory DW, Schaffner W, McGee ZA.** 1985. Tularemia: a 30-year experience with 88 cases. Medicine **64:**251–269. http://dx.doi.org/10.1097/00005792-198507000-00006.
6. **Cross JT, Schutze GE, Jacobs RF.** 1995. Treatment of tularemia with gentamicin in pediatric patients. Pediatr Infect Dis J **14:**151–152. http://dx.doi.org/10.1097/00006454-199502000-00014.
7. **Mason WL, Eigelsbach HT, Little SF, Bates JH.** 1980. Treatment of tularemia, including pulmonary tularemia, with gentamicin. Am Rev Respir Dis **121:**39–45.
8. **Pérez-Castrillón JL, Bachiller-Luque P, Martín-Luquero M, Mena-Martín FJ, Herreros V.** 2001. Tularemia epidemic in northwestern Spain: clinical description and therapeutic response. Clin Infect Dis **33:**573–576. http://dx.doi.org/10.1086/322601.
9. **Doyle TC, Burns SM, Contag CH.** 2004. *In vivo* bioluminescence imaging for integrated studies of infection. Cell Microbiol **6:**303–317. http://dx.doi.org/10.1111/j.1462-5822.2004.00378.x.
10. **Andreu N, Zelmer A, Sampson SL, Ikeh M, Bancroft GJ, Schaible UE, Wiles S, Robertson BD.** 2013. Rapid *in vivo* assessment of drug efficacy against *Mycobacterium tuberculosis* using an improved firefly luciferase. J Antimicrob Chemother **68:**2118–2127. http://dx.doi.org/10.1093/jac/dkt155.
11. **Contag CH, Contag PR, Mullins JI, Spilman SD, Stevenson DK, Benaron DA.** 1995. Photonic detection of bacterial pathogens in living hosts. Mol Microbiol **18:**593–603. http://dx.doi.org/10.1111/j.1365-2958.1995.mmi_18040593.x.
12. **Andreu N, Zelmer A, Fletcher T, Elkington PT, Ward TH, Ripoll J, Parish T, Bancroft GJ, Schaible U, Robertson BD, Wiles S.** 2010. Optimisation of bioluminescent reporters for use with mycobacteria. PLoS One **5:**e10777. http://dx.doi.org/10.1371/journal.pone.0010777.
13. **Bacconi M, Haag AF, Torre A, Castagnetti A, Chiarot E, Delany I, Bensi G.** 2016. A stable luciferase reporter plasmid for *in vivo* imaging in murine models of *Staphylococcus aureus* infections. Appl Microbiol Biotechnol **100:**3197–3206. http://dx.doi.org/10.1007/s00253-015-7229-2.
14. **Francis KP, Joh D, Bellinger-Kawahara C, Hawkinson MJ, Purchio TF, Contag PR.** 2000. Monitoring bioluminescent *Staphylococcus aureus* infections in living mice using a novel *luxABCDE* construct. Infect Immun **68:**3594–3600. http://dx.doi.org/10.1128/IAI.68.6.3594-3600.2000.
15. **Massey S, Johnston K, Mott TM, Judy BM, Kvitko BH, Schweizer HP, Estes DM, Torres AG.** 2011. *In vivo* bioluminescence imaging of *Burkholderia mallei* respiratory infection and treatment in the mouse model. Front Microbiol **2:**174. http://dx.doi.org/10.3389/fmicb.2011.00174.
16. **Nham T, Filali S, Danne C, Derbise A, Carniel E.** 2012. Imaging of bubonic plague dynamics by *in vivo* tracking of bioluminescent *Yersinia pestis*. PLoS One **7:**e34714. http://dx.doi.org/10.1371/journal.pone.0034714.
17. **Sun Y, Connor MG, Pennington JM, Lawrenz MB.** 2012. Development of bioluminescent bioreporters for *in vitro* and *in vivo* tracking of *Yersinia pestis*. PLoS One **7:**e47123. http://dx.doi.org/10.1371/journal.pone.0047123.
18. **Zhang T, Li S-Y, Nuermberger EL.** 2012. Autoluminescent *Mycobacterium tuberculosis* for rapid, real-time, non-invasive assessment of drug and vaccine efficacy. PLoS One **7:**e29774. http://dx.doi.org/10.1371/journal.pone.0029774.
19. **Rocchetta HL, Boylan CJ, Foley JW, Iversen PW, LeTourneau DL,**

AQ: E

McMillian CL, Contag PR, Jenkins DE, Parr TR. 2001. Validation of a noninvasive, real-time imaging technology using bioluminescent *Escherichia coli* in the neutropenic mouse thigh model of infection. Antimicrob Agents Chemother **45:**129–137. http://dx.doi.org/10.1128/AAC.45.1.129-137.2001.

20. **Slate AR, Bandyopadhyay S, Francis KP, Papich MG, Karolewski B, Hod EA, Prestia KA.** 2014. Efficacy of enrofloxacin in a mouse model of sepsis. J Am Assoc Lab Anim Sci **53:**381–386.
21. **van Staden ADP, Heunis T, Smith C, Deane S, Dicks LMT.** 20 June 2016. Efficacy of lantibiotic treatment of *Staphylococcus aureus*-induced skin infections, monitored by *in vivo* bioluminescent imaging. Antimicrob Agents Chemother http://dx.doi.org/10.1128/AAC.02938-15.
22. **Levy M, Antunes A, Fiette L, Deghmane A-E, Taha M-K.** 2015. Impact of corticosteroids on experimental meningococcal sepsis in mice. Steroids **101:**96–102. http://dx.doi.org/10.1016/j.steroids.2015.05.013.
23. **Bina XR, Miller MA, Bina JE.** 2010. Construction of a bioluminescence reporter plasmid for *Francisella tularensis*. Plasmid **64:**156–161. http://dx.doi.org/10.1016/j.plasmid.2010.07.001.
24. **LoVullo ED, Miller CN, Pavelka MS, Kawula TH.** 2012. TetR-based gene regulation systems for *Francisella tularensis*. Appl Environ Microbiol **78:**6883–6889. http://dx.doi.org/10.1128/AEM.01679-12.
25. **Flick-Smith HC, Commander NJ, Scott AE, Thomas RJ, Brown MA, Richards MI, Scott JC, Martin KR, Harding SV, Atkins HS.** 2016. Establishing an *in vivo* imaging capability in high containment. Appl Biosafety http://dx.doi.org/10.1177/1535676016631878.
26. **Wang X, Li Z, Li B, Chi H, Li J, Fan H, Yao R, Li Q, Dong X, Chen M, Qu H, Wang Y, Gao W, Wang Y, Sun Y, Sun R, Qian J, Xia Z.** 2016. Bioluminescence imaging of colonization and clearance dynamics of *Brucella suis* vaccine strain S2 in mice and guinea pigs. Mol Imaging Biol **18:**519–526. http://dx.doi.org/10.1007/s11307-015-0925-6.
27. **Hutchens M, Luker GD.** 2007. Applications of bioluminescence imaging to the study of infectious diseases. Cell Microbiol **9:**2315–2322. http://dx.doi.org/10.1111/j.1462-5822.2007.00995.x.
28. **Alam R, Karam LM, Doane TL, Zylstra J, Fontaine DM, Branchini BR, Maye MM.** 2014. Near infrared bioluminescence resonance energy transfer from firefly luciferase–quantum dot bionanoconjugates. Nanotechnology **25:**495606. http://dx.doi.org/10.1088/0957-4484/25/49/495606.
29. **Alam FM, Bateman C, Turner CE, Wiles S, Sriskandan S.** 2013. Non-invasive monitoring of *Streptococcus pyogenes* vaccine efficacy using biophotonic imaging. PLoS One **8:**e82123. http://dx.doi.org/10.1371/journal.pone.0082123.
30. **Bernthal NM, Stavrakis AI, Billi F, Cho JS, Kremen TJ, Simon SI, Cheung AL, Finerman GA, Lieberman JR, Adams JS, Miller LS.** 2010. A mouse model of post-arthroplasty *Staphylococcus aureus* joint infection to evaluate *in vivo* the efficacy of antimicrobial implant coatings. PLoS One **5:**e12580. http://dx.doi.org/10.1371/journal.pone.0012580.
31. **Maier TM, Havig A, Casey M, Nano FE, Frank DW, Zahrt TC.** 2004. Construction and characterization of a highly efficient *Francisella* shuttle plasmid. Appl Environ Microbiol **70:**7511–7519. http://dx.doi.org/10.1128/AEM.70.12.7511-7519.2004.
32. **Grady R, Hayes F.** 2003. Axe-Txe, a broad-spectrum proteic toxin-antitoxin system specified by a multidrug-resistant, clinical isolate of *Enterococcus faecium*. Mol Microbiol **47:**1419–1432. http://dx.doi.org/10.1046/j.1365-2958.2003.03387.x.
33. **Pomerantsev AP, Golovliov IR, Ohara Y, Mokrievich AN, Obuchi M, Norqvist A, Kuoppa K, Pavlov VM.** 2001. Genetic organization of the *Francisella* plasmid pFNL10. Plasmid **46:**210–222. http://dx.doi.org/10.1006/plas.2001.1548.
34. **Koncz C, Olsson O, Langridge WH, Schell J, Szalay AA.** 1987. Expression and assembly of functional bacterial luciferase in plants. Proc Natl Acad Sci U S A **84:**131–135. http://dx.doi.org/10.1073/pnas.84.1.131.
35. **Rolfe MD, Rice CJ, Lucchini S, Pin C, Thompson A, Cameron ADS, Alston M, Stringer MF, Betts RP, Baranyi J, Peck MW, Hinton JCD.** 2012. Lag phase is a distinct growth phase that prepares bacteria for exponential growth and involves transient metal accumulation. J Bacteriol **194:**686–701. http://dx.doi.org/10.1128/JB.06112-11.
36. **Nackerdien ZE, Keynan A, Bassler BL, Lederberg J, Thaler DS.** 2008. Quorum sensing influences *Vibrio harveyi* growth rates in a manner not fully accounted for by the marker effect of bioluminescence. PLoS One **3:**e1671. http://dx.doi.org/10.1371/journal.pone.0001671.
37. **Read HM, Mills G, Johnson S, Tsai P, Dalton J, Barquist L, Print CG, Patrick WM, Wiles S.** 2016. The *in vitro* and *in vivo* effects of constitutive light expression on a bioluminescent strain of the mouse enteropathogen *Citrobacter rodentium*. PeerJ **4:**e2130. http://dx.doi.org/10.7717/peerj.2130.
38. **Miller MA, Stabenow JM, Parvathareddy J, Wodowski AJ, Fabrizio TP, Bina XR, Zalduondo L, Bina JE.** 2012. Visualization of murine intranasal dosing efficiency using luminescent *Francisella tularensis*: effect of instillation volume and form of anesthesia. PLoS One **7:**e31359. http://dx.doi.org/10.1371/journal.pone.0031359.
39. **Rosenthal E, Zinn KR.** 2009. Optical imaging of cancer: clinical applications. Springer Science & Business Media, New York, NY.
40. **Zijlstra WG, Buursma A, Meeuwsen-van der Roest WP.** 1991. Absorption spectra of human fetal and adult oxyhemoglobin, de-oxyhemoglobin, carboxyhemoglobin, and methemoglobin. Clin Chem **37:**1633–1638.
41. **Glomski IJ, Piris-Gimenez A, Huerre M, Mock M, Goossens PL.** 2007. Primary involvement of pharynx and Peyer's patch in inhalational and intestinal anthrax. PLoS Pathog **3:**e76. http://dx.doi.org/10.1371/journal.ppat.0030076.
42. **Conlan JW, KuoLee R, Shen H, Webb A.** 2002. Different host defences are required to protect mice from primary systemic vs pulmonary infection with the facultative intracellular bacterial pathogen, *Francisella tularensis* LVS. Microb Pathog **32:**127–134. http://dx.doi.org/10.1006/mpat.2001.0489.
43. **Crane DD, Scott DP, Bosio CM.** 2012. Generation of a convalescent model of virulent *Francisella tularensis* infection for assessment of host requirements for survival of tularemia. PLoS One **7:**e33349. http://dx.doi.org/10.1371/journal.pone.0033349.
44. **D'Elia RV, Laws TR, Carter A, Lukaszewski R, Clark GC.** 2013. Targeting the "Rising DAMP" during a *Francisella tularensis* infection. Antimicrob Agents Chemother **57:**4222–4228. http://dx.doi.org/10.1128/AAC.01885-12.
45. **Conlan JW.** 2011. *Francisella tularensis*: a red-blooded pathogen. J Infect Dis **204:**6–8. http://dx.doi.org/10.1093/infdis/jir224.
46. **McCrumb FR.** 1961. Aerosol infection of man with *Pasteurella tularensis*. Bacteriol Rev **25:**262–267.
47. **Steiner DJ, Furuya Y, Metzger DW.** 2014. Host-pathogen interactions and immune evasion strategies in *Francisella tularensis* pathogenicity. Infect Drug Resist **7:**239–251. http://dx.doi.org/10.2147/IDR.S53700.
48. **Klimpel GR, Eaves-Pyles T, Moen ST, Taormina J, Peterson JW, Chopra AK, Niesel DW, Carness P, Haithcoat JL, Kirtley M, Nasr AB.** 2008. Levofloxacin rescues mice from lethal intra-nasal infections with virulent *Francisella tularensis* and induces immunity and production of protective antibody. Vaccine **26:**6874–6882. http://dx.doi.org/10.1016/j.vaccine.2008.09.077.
49. **Piercy T, Steward J, Lever MS, Brooks TJG.** 2005. *In vivo* efficacy of fluoroquinolones against systemic tularaemia infection in mice. J Antimicrob Chemother **56:**1069–1073. http://dx.doi.org/10.1093/jac/dki359.
50. **Rotem S, Bar-Haim E, Cohen H, Elia U, Ber R, Shafferman A, Cohen O.** 2012. Consequences of delayed ciprofloxacin and doxycycline treatment regimens against *Francisella tularensis* airway infection. Antimicrob Agents Chemother **56:**5406–5408. http://dx.doi.org/10.1128/AAC.01104-12.
51. **Barnes PD, Bergman MA, Mecsas J, Isberg RR.** 2006. *Yersinia pseudotuberculosis* disseminates directly from a replicating bacterial pool in the intestine. J Exp Med **203:**1591–1601. http://dx.doi.org/10.1084/jem.20060905.
52. **Roussey JA, Oliveira LJ, Langohr IM, Sledge DG, Coussens PM.** 10 March 2016. Regulatory T cells and immune profiling in Johne's disease lesions. Vet Immunol Immunopathol http://dx.doi.org/10.1016/j.vetimm.2016.03.008.
53. **Melton-Witt JA, Rafelski SM, Portnoy DA, Bakardjiev AI.** 2012. Oral infection with signature-tagged *Listeria monocytogenes* reveals organ-specific growth and dissemination routes in guinea pigs. Infect Immun **80:**720–732. http://dx.doi.org/10.1128/IAI.05958-11.
54. **Ojeda SS, Wang ZJ, Mares CA, Chang TA, Li Q, Morris EG, Jerabek PA, Teale JM.** 2008. Rapid dissemination of *Francisella tularensis* and the effect of route of infection. BMC Microbiol **8:**215. http://dx.doi.org/10.1186/1471-2180-8-215.
55. **Rossow H, Forbes KM, Tarkka E, Kinnunen PM, Hemmilä H, Huitu O, Nikkari S, Henttonen H, Kipar A, Vapalahti O.** 2014. Experimental infection of voles with *Francisella tularensis* indicates their amplification role in tularemia outbreaks. PLoS One **9:**e108864. http://dx.doi.org/10.1371/journal.pone.0108864.
56. **Schuijt TJ, Lankelma JM, Scicluna BP, de Sousa e Melo F, Roelofs JJTH, de Boer JD, Hoogendijk AJ, de Beer R, de Vos A, Belzer C, de Vos WM,**

van der Poll T, Wiersinga WJ. 2016. The gut microbiota plays a protective role in the host defence against pneumococcal pneumonia. Gut **65:** 575–583. http://dx.doi.org/10.1136/gutjnl-2015-309728.

57. **Romond M-B, Colavizza M, Mullié C, Kalach N, Kremp O, Mielcarek C, Izard D.** 2008. Does the intestinal bifidobacterial colonisation affect bacterial translocation? Anaerobe **14:**43–48. http://dx.doi.org/10.1016/j.anaerobe.2007.09.003.
58. **Lam LH, Monack DM.** 2014. Intraspecies competition for niches in the distal gut dictate transmission during persistent *Salmonella* infection. PLoS Pathog **10:**e1004527. http://dx.doi.org/10.1371/journal.ppat.1004527.
59. **Lim CH, Voedisch S, Wahl B, Rouf SF, Geffers R, Rhen M, Pabst O.** 2014. Independent bottlenecks characterize colonization of systemic compartments and gut lymphoid tissue by *Salmonella*. PLoS Pathog **10:** e1004270. http://dx.doi.org/10.1371/journal.ppat.1004270.

AUTHOR QUERIES

AUTHOR PLEASE ANSWER ALL QUERIES 1

AQau—Please confirm the given-names and surnames are identified properly by the colors. ■= Given-Name, ■= Surname

AQaff—Please confirm the following full affiliations or correct here as necessary. This is what will appear in the online HTML version:

[a]Bacterial Pathogenesis Research Group, College of Life and Environmental Sciences, University of Exeter, Exeter, United Kingdom
[b]CBR Division, Defence Science and Technology Laboratory, Porton Down, Salisbury, Wiltshire, United Kingdom

AQaff—This affiliation line will appear in the PDF version of the article and matches that on page 1 of the proof; corrections to this affiliation line may be made here **or** on page 1 of the proof:

Bacterial Pathogenesis Research Group, College of Life and Environmental Sciences, University of Exeter, Exeter, United Kingdom[a]; CBR Division, Defence Science and Technology Laboratory, Porton Down, Salisbury, Wiltshire, United Kingdom[b]

AQA—If transposition of "for imaging studies" not OK, please clarify.

AQB—OK to cite Fig. 2 here? Per ASM style, figures must be cited in numerical order in the text.

AQC—If "beginning" not as meant, please clarify what "at the onset" relates to.

AQD—If "causes in bacteria" not OK, please reword. Changed because "confer" has a positive connotation, and attenuation may not be positive for bacteria.

AQE—Correct that this is about a single mouse? or mice? presumably not the same mouse discussed in the last paragraph of Results, who succumbed by day 19?

AQF—Please check sentence beginning "Treatment is terminated."

AQG—If not the regions, please clarify what are presumed to be Peyer's patches.